Accuracy of *K*-shell spectra modeling in high-density plasmas

S. H. Glenzer, K. B. Fournier,[1] C. Decker,[1] B. A. Hammel,[1] R. W. Lee,[1] L. Lours,[2] B. J. MacGowan,[1] and A. L. Osterheld[1]
[1]*L-437, Lawrence Livermore National Laboratory, University of California, P. O. Box 808, Livermore, California 94551*
[2]*CEA/DAM-Ile de France, Boîte Postale 12, 91680 Bruyères-le-Châtel, France*
(Received 4 February 2000)

We present spectroscopic measurements of the helium-like and lithium-like argon emission supported by Thomson scattering diagnostics on gas bag targets. These data provide critical tests of plasma spectroscopic *K*-shell models. In particular, we have measured the line radiation in the wavelength region of the He-like Ar $1s^2-1s3l$ transition (He-β) that is of interest for density and temperature measurements of plasmas from gas-filled targets ($n_e \leqslant 10^{21}$ cm^{-3}), laser ablation targets ($n_e \leqslant 10^{22}$ cm^{-3}), and inertial confinement fusion capsule implosions ($n_e \geqslant 10^{24}$ cm^{-3}). The spectra show lithium-like dielectronic satellites on the red wing of the He-β line that are temperature sensitive and are known to influence the shape of the Stark-broadened line profiles observed from implosions. To examine the kinetics modeling of this complex, i.e., the He-β and its associated satellites, we have performed experiments in gas bag plasmas at densities of $(0.6–1.1)\times 10^{21}$ cm^{-3} where we independently determine the electron temperature with ultraviolet Thomson scattering. The comparison of the satellite intensities with kinetics modeling shows good agreement for satellites whose upper states are populated by dielectronic capture, but shows discrepancies for inner-shell collisional excited transitions.

PACS number(s): 52.70.La, 32.30.Rj, 52.25.Qt, 52.25.Nr

I. INTRODUCTION

Because of the high electron densities encountered in laser-driven inertial confinement fusion research, x-ray spectroscopy is often applied to measure the plasma conditions in fusion capsule implosions [1–10] and in the laser-produced plasmas surrounding the capsule [11,12]. In current indirect drive experiments, capsule implosions driven by x rays from high-Z hohlraums converge to a final radius that is less than 0.1 of the original radius (275 μm). Consequently, plasma conditions similar to those of stars, i.e., extremely high densities $n_e = 10^{24}$ cm^{-3} and temperatures $T_e = 1–2$ keV, have been produced [6]. The characterization of these dense plasmas requires x ray emission or neutron diagnostics [13]. In particular, the spectrum of the $1s^2\,{}^1S-1s3p\,{}^1P^o$ of Ar XVII (He-β) with its dielectronic satellites arising from the Li-like Ar states $1s^2n\ell-1sn\ell n'\ell'$, referred to below as the He-β complex, has been found to be a valuable diagnostic of electron densities and temperatures [6,14,15]. This line is Stark broadened so that densities can be inferred from the width of the spectral line, and the upper levels of the observable dielectronic satellites on the red wing of the He-β line are predominantly populated by dielectronic recombination so that their relative intensity is sensitive to the electron temperature [16,17]. Some of the higher-*n* satellite features overlap with the He-β transition and consequently need to be self-consistently included in the fit of the whole line shape with a Stark-broadening code coupled to a kinetics (collisional-radiative) model [14,18]. This procedure applies kinetics modeling to very high densities where the codes have not been tested against independent measurements. In this study, we perform critical comparisons of various kinetics calculations with experimental data from well-characterized plasmas at the highest possible densities where optical diagnostics, i.e., Thomson scattering, can be used to independently measure the plasma conditions. This is a necessary first step toward a critical evaluation of the diagnostic procedures used at the highest measured plasma density of $>10^{24}$.

The present study was particularly motivated by observations of unexpectedly strong dielectronic satellite emission in recent implosion experiments. For example, the temporally resolved measurements [14] of the spectrum of the He-β line plus satellites from indirectly driven implosions have resulted in the diagnostic of peak temperatures of ~ 0.8 keV, which is lower by about a factor of two [6] than those calculated with two-dimensional hydrodynamic modeling using the code LASNEX [19]. Moreover, some experiments with directly driven capsules show dielectronic satellites that completely dominate the spectrum at late times in the implosion [20]. To test the accuracy of the kinetics models and to rule out that the interpretation of the implosion data is affected by deficiencies in the models, we have performed new experiments in well-characterized gas bag plasmas [21–23] at densities $n_e = 0.6\times 10^{21}$ cm^{-3} and $n_e = 1.1\times 10^{21}$ cm^{-3} (see Sec. II). These gas bag plasmas are homogeneous and independently diagnosed with stimulated Raman scattering [22], x-ray spectroscopy [23], and temporally resolved Thomson scattering (see Sec. III). In particular, the Thomson scattering diagnostic gives electron temperature data consistent with hydrodynamic modeling suggesting that gas bag plasmas are suitable sources to test our kinetics modeling capability.

To compare the experimental spectra with synthetic spectra, we employed the HULLAC suite of kinetics codes [24–28]. In addition, we make comparisons with calculations in the corona approximation employing atomic data from various authors [26,29–31]. We find for the two different electron densities that the kinetics modeling accurately predicts the relative intensity of the measured Li-like dielectronic capture satellite transitions and of the He-β transition, which consists of the sum of the resonance line (He-β_1:

$1s^2\,{}^1S_0-1s3p\,{}^1P_1^o$) and the less intense intercombination line from the triplet to the singlet system of He-like argon (He-β_2: $1s^2\,{}^1S_0-1s3p\,{}^3P_1^o$). Spectral line emission originating from levels whose population is primarily determined by electron collisional processes, on the other hand, shows discrepancies of up to a factor of two compared to the modeling. This is observed for inner-shell excited satellite transitions as well as for the ratio of the intercombination to the resonance line.

Such discrepancies have also been reported previously from low density tokamak plasma experiments [32] at densities 10^7 smaller than the current gas bag plasmas. On the other hand, in the present study we observe better agreement between spectral calculations and the experimental dielectronic capture satellite emission than in the previous tokamak study [32]. This finding could be related to improved diagnostics in the present study, i.e., Thomson scattering versus electron cyclotron resonance emission, reduced plasma gradients, i.e., the gas bag plasma source versus a tokamak plasma, and to improvements in the spectral modeling (described in Sec. IV below). Moreover, the study of Ref. [33] has shown similar discrepancies of experimental inner-shell collisional excited satellites and calculations in the coronal approximation. However, these experiments lack an independent temperature diagnostic and measure time-integrated spectra from rather inhomogeneous laser-produced blow-off plasmas making a quantitative comparison with kinetics modeling difficult.

Our simultaneous temporally resolved measurements of Thomson scattering and x-ray spectra test the kinetics models at densities about three orders of magnitude lower than those of fusion capsule implosions, but seven orders of magnitude above those of previous studies [32,34]. In spite of the remaining discrepancies between calculated and measured inner-shell satellite intensities, the fact that the strongest satellite features, i.e., the dielectronic capture satellites, are well modeled by the HULLAC code may affect the interpretation of ICF capsule implosion experiments. Our findings indicate that we should revisit the analysis of the higher density implosions to find if the kinetics modeling is consistent with the results obtained here. Moreover, having proven the technique to benchmark kinetics calculations in laser-produced plasma conditions, one can hope to extend this method to verify critically important aspects of indirectly driven capsule physics by testing the conditions created inside hohlraums.

II. EXPERIMENT

A. Gas bag and laser parameters

Gas bags consist of two 0.35 μm thick polyimide ($C_{14}H_6O_4N_2$) membranes that are mounted on either side of a 0.4 mm thick aluminum washer with an inner diameter of 2.75 mm. The membranes in this study are inflated by propane (C_3H_8) or neopentane (C_5H_{12}) plus a small amount of argon (1% by atomic number in each case) as spectroscopic test element. The gas concentrations are measured by mass spectrometry for each batch of mixed gas. The gas pressure is kept at one atmosphere by monitoring that results in a nearly spherical balloon target of 2.75 mm $\times$ 2.5 mm with a known atomic density. Figure 1 shows an image of the target where one can see the vertical slits that are mounted for the spatially resolving x-ray spectroscopic measurements.

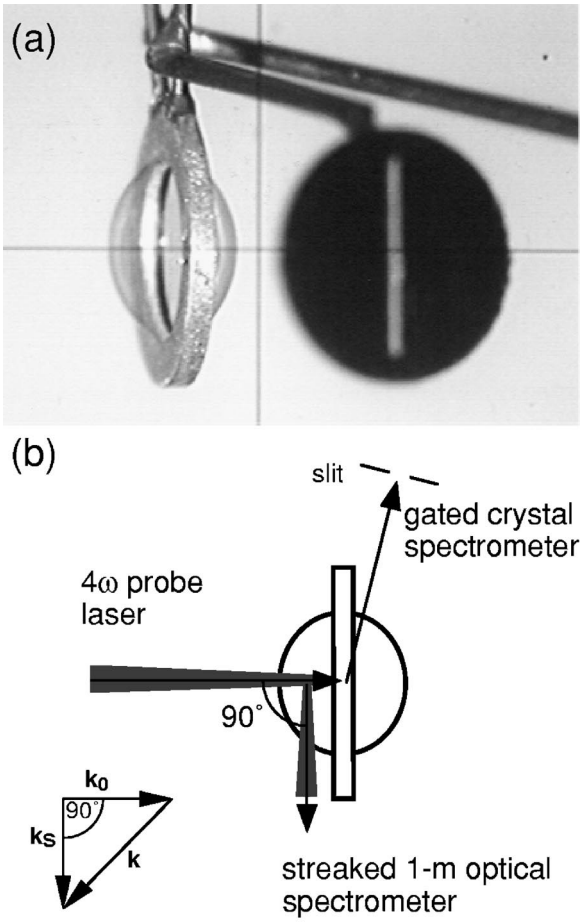

FIG. 1. Gas bag target before it is pressurized with C_3H_8 or C_5H_{12}. Two vertical slits have been mounted on this target at a distance of 8 mm from gas bag center. The thickness and the inner diameter of the washer is 0.4 and 2.75 mm, respectively (a). Also shown is a schematic of the 4ω probe laser and the 4ω Thomson scattering detection system with a **k**-vector diagram, as well as the viewing angle of the x-ray crystal spectrometer (b).

The gas bags are heated with nine beams of the Nova laser [35], a Nd: glass laser operating at 1.055 μm. For the heating of gas bags, the laser light is frequency tripled to $\lambda = 351.1$ nm. Focusing optics of $f/4.3$ are used with a defocus of 6.78 mm. This configuration results in laser beams converging at the center of the gas bags with a laser spot size of each individual beam of ~ 1.7 mm diameter on the surface of the gas bag [21]. A total energy of 21 kJ is delivered in a 1 ns square pulse giving an averaged intensity of 10^{14} W cm^{-2} per beam.

Gas bag targets convert most of the incident laser energy into thermal energy of the electrons and less into the kinetic energy of bulk plasma motion than irradiation of a solid target. Thus, a high-temperature, high-density plasma is produced with temperature and density gradients that have been measured with optical and x-ray diagnostics and are found to be small (see Sec. III). When compared with conventional sources such as laser-produced blow-off plasmas, exploding foils, or tokamak plasmas these characteristics make gas bags a suitable source for plasma spectroscopic studies.

B. Diagnostics configuration

Figure 1(b) shows a schematic of the two main diagnostics employed to measure x-ray spectra using a crossed slit configuration and temperatures with 4ω Thomson scattering. The spectroscopic measurements have been performed with a crystal spectrometer coupled to a gated microchannelplate detector (MCP). The x-ray emission is observed through a slit of 3 mm height and 150 μm width cut in a copper shield (300 μm thick, 3.2 mm diameter) and mounted on the target at a distance of 8 mm, effectively limiting the plasma size seen by the spectrometer [Fig. 1(a)]. This slit allows a view through the gas bag center. At a distance of 11.9 cm from the first slit we used four parallel slits (250 μm width, 2 mm height) to image the emission onto four parallel strips of a gated MCP detector with a factor of two magnification. Between the four slits and the MCP a pentaerythritol (PET) crystal is mounted at the Bragg angle to spectrally disperse the plasma emission. Since source broadening is efficiently reduced by the first slit, a resolution of $\lambda/\Delta\lambda = 800$ is achieved by this type of spectrometer [36].

The gated MCP detector [37,38] has four active rectangular strips (4 mm$\times$40 mm). A square gate pulse of 0.08 ns traverses the length of the strip along the wavelength dispersion direction in 0.25 ns. At the output of the MCP a P20 phosphor is mounted, and its illumination is recorded on film (Kodak TMAX 3200) that is digitized with a resolution of 22 μm. The gate pulse results in a time resolution of 0.1 ns for the measurements of the He-β complex, i.e., because the lines of interest are only a few millimeters apart on the MCP. We have chosen a time delay of 0.25 ns between the strips, but in all cases, data from a maximum of only two strips were timed properly to achieve a good signal to noise ratio of the satellite emission. Therefore, data from 32 shots have been accumulated and used for the data analysis.

For Thomson scattering, we employed a 50 J 4ω probe laser (operating wavelength: $\lambda_0 = 263.3$ nm) [39]. Early experiments with 2ω and 3ω lasers have shown that a short-wavelength probe is required to characterize open geometry large-scale length ICF plasmas, because of strong laser light absorption, stray light as well as stimulated Raman side scattering from the heater beams in the wavelength range around 2ω and 3ω. We focus the probe laser into the gas bag target to a spot of 60 μm$\times$120 μm. It results in a 4ω intensity of $>3\times10^{14}$ W cm^{-2} (at 4ω) that was shown, in separate experiments, to not influence the plasma as long as it is hot and heated by kJ laser beams. The pointing accuracy of the 4ω probe laser has been demonstrated to be 100 μm by taking x-ray images from the 4ω probe together with the emission through five backlit fiducial holes that were absolutely positioned prior to the shots to within 10 μm.

The Thomson scattered light has been imaged at an angle of 90° with $f/10$ optics onto the entrance slit of a 1 m (SPEX) spectrometer. We employed an S-20 streak camera to record spectra with a temporal resolution of 30 ps and a wavelength resolution of 0.05 nm. A magnification of 1.5 together with the use of a 200 μm spectrometer entrance slit width, and 100 μm streak camera slit width, yields a cylindrical scattering volume of $\sim$70 μm in horizontal and $\sim$120 μm in vertical direction. This scattering volume is small compared to the size of the plasma. The choice of the probe laser wavelength of 263 nm and of the scattering angle of 90° results in collective Thomson scattering [40,41] from fluctuations characterized by wave numbers $\mathbf{k}$ [cf. Fig 1(b)] such that the scattering parameter is $\alpha = 1/k\lambda_D > 2$ for the gas bag electron densities and temperatures. The Thomson scattering spectra are dominated by the narrow ion feature which shows scattering resonances at the ion acoustic wave frequencies shifted from the incident probe laser frequency on either side on the frequency scale (redshift and blueshift for copropagating and counterpropagating waves along the scattering vector $\mathbf{k}$) containing the information on T_e and T_i of the plasma [39].

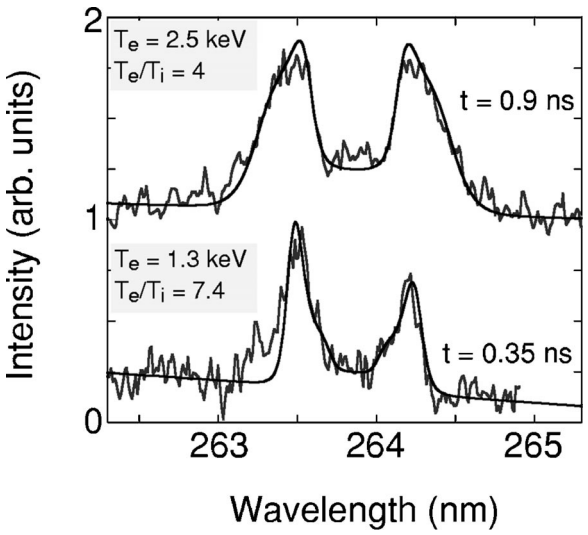

FIG. 2. Experimental Thomson scattering spectra from a C_5H_{12}-filled gas bag measured from a radial distance of 0.8 mm from the gas bag center. The spectra taken at $t = 0.35$ ns and $t = 0.9$ ns with a resolution of 30 ps show increasing electron temperatures and decreasing electron to ion temperature ratios. The parameters are inferred from the theoretical fits to the experimental data.

Additional diagnostics has been fielded on these experiments. They include a curved gated crystal spectrometer to obtain survey spectra, two gated pinhole (10 μm) cameras for two dimensional x-ray images, an x-ray streak camera for one-dimensional imaging with improved time resolution, and a crystal streak spectrometer monitoring the reproducibility of the argon emission. Data from these detectors have been discussed in more detail in Ref. [23].

III. PLASMA CHARACTERIZATION

To characterize the gas bags plasma temperature, density, and flow, we have applied Thomson scattering, Raman scattering, and standard He-$\alpha/jk\ell$ x-ray spectroscopic techniques. Thomson scattering observes the scattering of electromagnetic radiation from a probe laser by the electrons of the plasma. It is a spatially and temporally resolving technique whose interpretation is based on theory [42]. In the collective scattering regime, where the wavelength of the probe laser is larger than the Debye screening length, the collective behavior of the plasma is observed. In this case, the scattered light shows resonances at the ion acoustic and electron plasma wave frequency. From the measured wavelengths and damping of these features, called ion and elec-

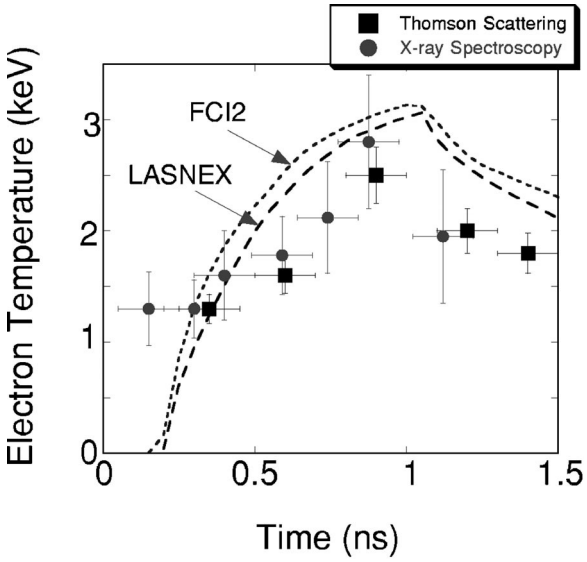

FIG. 3. Electron temperature of a C_5H_{12}-filled gas bag as function of time measured from a radial distance of 0.8 mm from gas bag center. The Thomson scattering data are in excellent agreement with the x-ray spectroscopic measurements using the standard ratio of the He-α to the $jk\ell$ dielectronic satellite transitions. The experiments are also consistent with two-dimensional hydrodynamic modeling using the codes LASNEX and FCI2.

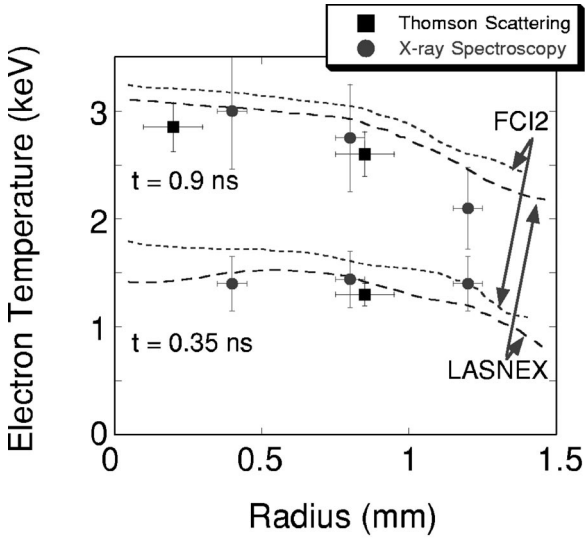

FIG. 4. Experimental electron temperature data for various radial positions measured at $t=0.35$ ns and $t=0.9$ ns. The temperatures from Thomson scattering show excellent agreement with the results from x-ray spectroscopy. At $t=0.35$ ns the electron temperature profile is flat indicating the utility of gas bags for spectroscopic investigations.

tron features, respectively, one obtains the electron temperatures T_e and densities n_e, ion temperatures T_i, and the averaged ionization stage Z. Furthermore, the macroscopic flow velocities V can be inferred from the Doppler shift of the spectra [39].

Figure 2 shows examples of two Thomson scattering spectra of the ion feature measured at a distance of 800 μm from gas bag center at $t=0.35$ ns and $t=0.9$ ns. Two ion acoustic resonances are clearly identified. Each peak consists of two unresolved ion acoustic waves, one belonging to carbon (slow mode) and one belonging to hydrogen (fast mode) [39,43]. With increasing time, the ion acoustic peaks show increased separation and broadening indicating increasing electron and ion temperatures during the heating of the gas bag plasma. To accurately infer temperatures from these spectra, we convolute the form factor $S(\mathbf{k},\omega)$ for multi-ion species [44] with the experimental instrument function and fit the resulting profile to the data. Examples of these fits are also shown in Fig. 2. We obtain an error estimate for the electron temperature of $<10\%$ from the fitting procedure by varying the calculated profile within the noise of the experimental data.

The experimental electron temperatures show mutual agreement between the results from the temporally and spatially resolved Thomson scattering technique and with temporally and spatially resolved x-ray spectroscopy using the intensity ratio of the He-like Ar $1s^2-1s2l$ (He-α) line to the lithium-like $jk\ell$ dielectronic satellites [23]. This intensity ratio has many advantages over other spectroscopic techniques: the lines can easily be made optically thin by adjusting the impurity concentrations; the lines are separated only by a small wavelength interval so that the sensitivity of the instrument does not change drastically reducing errors due to the relative calibration; and the upper states of the dielectronic satellite transitions are populated on time scales of 100 ps so that there are only small differences in the time resolved and steady state analysis of the spectra reducing possible errors even further. The two techniques are compared in Fig. 3 together with LASNEX and FCI2 simulations (discussed below) at a distance of 800 μm from the gas bag center. The error bars for the spectroscopically derived temperatures are in the range of 15%–20% depending on the noise amplitude of the individual spectra at various times. The Thomson scattering data are accurate to within 10%. We find agreement between these two diagnostic methods. In separate gas bag experiments, we have also found that the temperatures inferred with the dielectronic satellite technique compare well to the isoelectronic ratio [11,45,46] of the He-β lines of argon and chlorine [23]. Moreover, the experimental data are in reasonable agreement with the simulations. For this comparison, we include the heater beam scattering losses by SBS and SRS. The simulations show higher peak temperatures and also a faster rise of the electron temperature than experimentally observed.

Figure 4 shows the temperatures derived from the Thomson scattering and from the observed ratio of the emission of the He-α to its satellites along with those temperatures predicted by hydrodynamic simulations as function of the gas bag radius. At the time of the measurements of the He-β transition plus satellites, i.e., 0.3 ns$<t<$0.5 ns, we find that gas bag plasmas are homogeneous, $\Delta T_e/\Delta R<20\%$. At the time close to peak temperature, i.e., $t=0.9$ ns, we find a homogeneous center with a diameter of 2 mm, $\Delta T_e/\Delta R<30\%$.

Two dimensional, cylindrically symmetric hydrodynamic simulations of the gas bags were performed with the radiation-hydrodynamic codes LASNEX and FCI2. Both of these codes employ ray tracing techniques to model laser propagation and include inverse bremsstrahlung for laser absorption. Laser scattering losses of about 20% were assumed

[47]. Electron heat transport assumed to be dominated by diffusion and the heat flux is constrained via a flux limit in both codes. Although these two codes have treated the same physical processes, the details of the implementation of the physcial approximations, as well as the details of the discretization of the problem, may differ. For this reason, using two different codes offers a more robust comparison.

The laser beam pattern incident on the gas bag is inherently three dimensional. Although, the beams are defocused such that the entire gas bag is irradiated, there are regions of beam overlap resulting in variations in the laser intensity. In addition, all of the beams have holes in them due to a beam block positioned in the center of each beam. This results in 3D inhomogeneities that cannot be modeled by a 2D simulations. In order to see the effects of nonuniform beam heating we have simulated beam overlap and holes in 2D simulations. These effects were simulated by irradiating the gas bag with rings. The results were that the simulated nonuniform heating produced regions where the temperature fell off with radius more rapidly than it does for uniform heating. Therefore, we believe that the measured temperature gradient at $t=0.9$ ns should, indeed, be larger than the simulated gradient (see Fig. 4). We intend to examine this problem with three dimensional simulations in the future using the realistic laser beam profiles.

In addition to the discrepancies between data and simulations, we find that the two simulations results are not identical. First, although both codes use flux limited diffusion the method in which it is employed differs. In diffusive heat transport the heat flux Q is given by the well know Spitzer–Härm formula $Q_{\mathrm{SH}}=-\kappa\nabla(k_BT_e)$, where k_B is the Boltzmann constant. In regions of large temperature gradients this flux can be greater than the free streaming flux $Q_{fs}=n_ek_BT_eV_{th}$ which is unphysical. Therefore, when this condition occurs the heat flux used is some fraction f of the free streaming flux. The quantity f is referred to as the flux limiter. In LASNEX this is done by choosing $Q=\min(Q_{SH},fQ_{fs})$, whereas in FCI2 this is done by a harmonic average, i.e., $1/Q=1/Q_{\mathrm{SH}}+1/(fQ_{fs})$.

While the electron and ion temperatures in these gas bag plasmas are well known from the measurements described above, the electron density is principally known by the density of the gas fill. Measurements of the wavelength of the Raman scattered light which occurs at the frequency of the electron plasma or Langmuir wave give a value for the electron density which are consistent with the gas fill density [22]. The line intensity ratio of the He-α and intercombination line of helium-like argon have also been shown to be in agreement with the expected densities [23]. In summary, the detailed measurements and the general agreement with the simulations indicate that the plasma conditions in these gas bag targets are known so that it provides a spectroscopic test bed for kinetics codes.

IV. THEORY

A. Atomic data and kinetics models

Ab initio atomic structure data for the lithium-, helium-, and hydrogen-like isoelectronic sequences of Ar have been generated using the HULLAC suite of codes. The atomic data from HULLAC are used to calculate the full collisional-radiative model for highly stripped argon ions. All singly and doubly excited energy levels with principal quantum number $n \leqslant 5$ have been treated. (Some triply excited levels in the Li-like ion are considered, these configurations can be neglected in models at the densities of the present experiments.) The HULLAC package includes ANGLAR, which uses the graphical angular recoupling program NJGRAF [24] to generate fine structure levels in a jj-coupling scheme for a set of user-specified electron configurations. HULLAC then generates atomic wave functions using the fully relativistic, parametric potential code RELAC [25,26]; RELAC calculates the full multiconfiguration, intermediate coupled level energies, and radiative transition rates. RELAC also computes semirelativistic autoionization transition rates [27] to the ground and excited levels of an adjacent ion. The CROSS [28] suite of codes in the HULLAC package uses the factorization theorem of Bar-Shalom, Klapisch, and Oreg to compute the distorted wave approximation (DWA) electron-impact excitation rates between all levels of each charge state mentioned above.

The ionic transition rates above, including the autoionization rates from the Li- to He-like and He- to H-like ions, as well as direct, impact ionization and radiative recombination rate coefficients, are used to construct the collisional-radiative rate matrix

$$\frac{dn_j}{dt}=\sum_i n_iR_{i\rightarrow j}-n_j\sum_i R_{j\rightarrow i}, \tag{1}$$

where n_j is the population in level j, and $R_{i\rightarrow j}$ is the total rate for transitions between level i and j, possibly belonging to a neighboring isoelectronic sequence. The inverse of each ionization process, namely dielectronic recombination and three body recombination have been found according to the principle of detailed balance. Radiative recombination from and collisional ionization to the bare nucleus Ar^{18+} is also included in the rate matrix; the relative populations of the four charge states and the population in each level of each ion are then found in the steady state. The resulting collisional-radiative line emission, ε_{ij}, for each H-, He-, and Li-like transition from level i to level j, is found (in photons $\mathrm{s}^{-1}\,\mathrm{cm}^{-3}$) at the specific transition wavelength, λ_0, for a given temperature and density,

$$\varepsilon_{ij}(\lambda_0)=n_iA_{ij}, \tag{2}$$

where n_i is the (relative) population in the upper level and A_{ij} is the radiative transition rate from level i to level j. The He-β transitions has been checked for self-absorption effects in a self-consistent manner using the escape factor approximation [48]. The He-α and the He-β lines have been found to be optically thin for a spherical plasma with an electron density of $n_e=1.1\times10^{21}$ cm^{-3}, electron temperatures of 1.0 and 1.5 keV, ion temperatures of 1.0 keV, a 1% concentration of argon in C_5H_{12}, and a diameter of 2.5 mm. To produce a spectrum that can be compared to the experiment the calculated line intensities are convolved with a Gaussian instrument profile, ϕ, with a full width at half maximum equal to the resolution of the crystal spectrometer

$$\varepsilon(\lambda)=\sum_{ij}\varepsilon_{ij}(\lambda_0)\phi(\lambda), \tag{3}$$

where the sum is over all transitions in the model. An example of the calculated spectrum at $T_e=1.3$ keV and $n_e=1.1\times10^{21}$ cm^{-3} is shown in Fig. 5(c). The blended line intensities are integrated in wavelength

$$\varepsilon=\int\varepsilon(\lambda)d\lambda \tag{4}$$

in order to produce the ratio of Li- to He-like intensity listed in the HULLAC column in Table I, which are discussed in Sec. V.

B. Inner shell and DR satellites

In the low density limit, i.e., the coronal approximation, the lithium-like satellites to the helium-like resonance lines investigated here can be created by two mechanisms, inner shell electron impact excitation followed by radiative stabilization

$$1s^2n\ell+e\rightarrow1sn\ell n'\ell'^{*}+e\rightarrow1s^2n\ell+\gamma \tag{5}$$

or dielectronic recombination from the helium-like ion,

$$1s^2+e\rightarrow1sn\ell n'\ell'^{*}\rightarrow1s^2n\ell+\gamma, \tag{6}$$

where $1sn\ell n'\ell'^{*}$ is a doubly excited autoionizing lithium-like level, $1s^2n\ell$ is a stable lithium-like level, and γ is the observed photon. For the specific transitions observed in the present work, $n=2$ and $n'=3$ in Eqs. (5) and (6). The emissivity of a line from level j of ion Z excited by inner shell electron impact excitation is given by

$$\varepsilon_{\mathrm{IS}}=N_eN_ZC(T_e)\beta^R_{j,f}, \tag{7}$$

where N_e and N_Z are the electron and ion densities, $C(T_e)$ is the impact excitation rate coefficient and $\beta^R_{j,f}$ is the radiative branching ratio from the upper level of the observed transition,

$$\beta^R_{j,f}=\frac{A^R_{j,f}}{\Sigma_iA^A_{j,i}+\Sigma_fA^R_{j,f}}. \tag{8}$$

The sum over i in Eq. (8) runs over all levels in the next higher ion reachable from level j by autoionization, and the sum over f runs over all bound levels reachable from j by radiative decay.

The emissivity $\varepsilon_{\mathrm{DR}}$ of a lithium-like satellite excited by dielectronic recombination can be expressed as

$$\varepsilon_{\mathrm{DR}}=N_eN_{\mathrm{He}}F_1(T_e)F_2(j,f), \tag{9}$$

where all the temperature dependence is contained in

$$F_1(T_e)=\frac{1}{2}\left(\frac{4\pi a_0^2R}{T_e}\right)^{3/2}\exp(-\Delta E_{i,j}/T_e), \tag{10}$$

where a_0 is the Bohr radius, R is the Rydberg unit of energy, and $\Delta E_{i,j}$ is the capture energy of the free electron, i.e., the energy difference between the $1s^2$ level and a $1sn\ell n'\ell'^{*}$ level. The satellite intensity factor due to dielectronic recombination from level i of ion $(Z+1)$ via level j of ion Z to level f is given by

$$F_2(j,f)=\frac{g_j}{g_i}A^A_{j,i}\beta^R_{j,f}, \tag{11}$$

where the g's are the statistical weights of the intermediate

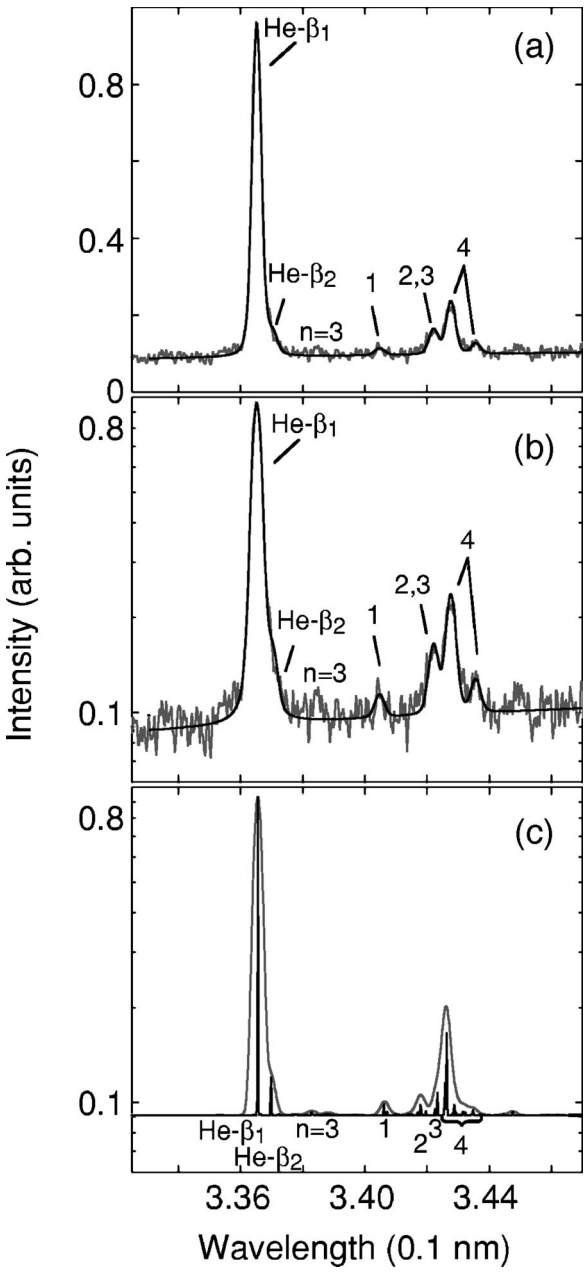

FIG. 5. High resolution spectra of the He-β transitions plus the $n=2$ (features 1 through 4) and $n=3$ dielectronic satellites measured at $t=0.35$ ns from a C_5H_{12}-filled gas bag (a). Also shown is the fit to the experimental data that is applied to determine the relative intensities of the spectral lines. The same data are also shown with a logarithmic scale (b). Synthetic spectra using the code HULLAC for the independently measured parameters $T_e=1.3$ keV and $n_e=1.1\times10^{21}$ cm^{-3} are shown for comparison with different resolution (c).

TABLE I. Comparison of the experimental line ratio, EXP, of the dielectronic satellite feature 4, $1s^22p-1s2p(^3P)3p$ to the He-β transition, I(4)/I(He-β_1+He-β_2), of Ar XVII with kinetics codes, HULLAC, RELAC [26], Safranova [29], Chen [30], and Nilsen [31] for various plasma conditions.

Ion	Temperature (keV)	Density (10^{21} cm^{-3})	Expt.	HULLAC	RELAC	Safranova	Chen	Nilsen
Ar XVII	1.25±15%	1.11±10%	0.20±5%	0.168	0.225	0.235	0.214	0.208
(C_5H_{12})	1.30±15%	1.11±10%	0.17±5%	0.158	0.207	0.216	0.197	0.193
Ar XVII	1.27±15%	0.63±10%	0.21±5%	0.180	0.218	0.226	0.207	0.201
(C_3H_8)	1.33±15%	0.63±10%	0.17±5%	0.166	0.199	0.207	0.189	0.184
	1.48±15%	0.63±10%	0.12±5%	0.129	0.160	0.166	0.152	0.148

(autoionizing) and initial (recombining) levels, and $A^A_{j,i}$ is the rate of autoionization from level j to level i.

In the limit where all the excitation arises from the He $1s^2$ state a lithium-like dielectronic satellite line ($j\rightarrow f$) and the corresponding helium-like resonance line (W_n) can be used as a convenient temperature diagnostic of the local plasma conditions by dividing Eq. (9) by Eq. (7),

$$\frac{\varepsilon^{jf}_{\mathrm{DR}}}{\varepsilon^{W_n}_{\mathrm{IS}}}=\frac{F_1(T_e)F_2(j,f)}{C_{W_n}(T_e)}, \tag{12}$$

where the branching ratio for the helium-like resonance line is assumed to be one. This ratio is independent of the ionization balance between the He- and Li-like ions, and is also independent of the electron density. For the densities of tokamak plasmas [32,34], Eq. (12) is a good approximation of the satellite to resonance line intensity ratio. We compare the diagnostic ratio computed by Eq. (12) using the atomic data generated *ab initio* with RELAC [26,27] to the same ratio computed with the atomic data of Safronova [29], Chen [30], and Nilsen [31]. Results for the $1s^22p-1s2p(^3P)3p$ satellite transitions normalized to the He-β transition are shown in Table I. All four calculations agree to approximately ±10% around their average value at the temperatures of the present experiments.

We have integrated the collisional-radiative intensity of the line transitions (Sec. IV A) because our calculations show that a non-negligible flux of population into the upper levels of the dielectronic Li-like satellite lines, and to a lesser extent the upper levels of He-β, arrives via collisional transfer from levels other than the ground level of the He-like ion. Thus, the ratios are dependent on electron density and the relative populations of the He- and Li-like ions. At the densities of the present experiments, all four of the Li-like satellite features that we analyze [$1s^22s-1s2s(^1S)3p$ and $1s^22s-1s2s(^3S)3p$, labeled 1 and 3 by Beiersdorfer [32], fed primarily by collisional excitation, and $1s^22p-1s2p(^1P)3p$ and $1s^22p-1s2p(^3P)3p$, labeled 2 and 4 by Beiersdorfer [32], fed primarily by dielectronic recombination] are affected by collisional transfer of population from excited levels. The collisional-radiative ratios for the dielectronic satellite lines to He-β are more than 25% smaller than the diagnostic ratios found considering pure He-like ground level excitations. These two calculations are contrasted in the columns labeled HULLAC and RELAC, respectively, in Table I.

V. EXPERIMENTAL RESULTS AND DISCUSSIONS

A. Lithium-like satellite emission

Figure 5 shows an example of an x-ray spectrum in the wavelength region 0.332 nm$<\lambda<$0.345 nm measured at $t=0.3$ ns from a gas bag filled with C_5H_{12} and 1% Ar. The data have been measured spatially resolved along the slit and averaged over the region $r<1.2$ mm to reduce noise. The averaging is justified because at the time of the measurements the gas bag plasma is homogeneous as shown in Sec. III. The spectrum has been corrected for the wavelength dependent instrument response [49], filter transmission, and crystal reflectivity [50].

The spectrum is dominated by the $1s-3p$ resonance line of helium-like argon Ar XVII at $\lambda=0.3364$ nm, He-β_1, the theoretical transition energy of which has been used to determine the absolute wavelength scale of Fig. 5. A number of spectroscopic features can be identified on the red wing of He-β_1 that can be easily seen on the logarithmic scale provided in Fig. 5(b). These are the intercombination lines at $\lambda=0.337$ nm, He-β_2; dielectronic satellites with a $n=3$ spectator electron at $\lambda=0.3381$ nm; four satellite features with an $n=2$ spectator electron labeled 1 through 4 according to Ref. [32]. Feature 1 is observed at $\lambda=0.3407$ nm. Features 2 and 3 are not resolved with the present spectrometer and are observed at $\lambda=0.3422$ nm. Feature 4 is found at $\lambda=0.3428$ nm. The experimental wavelengths agree closely with the previous high-resolution measurements of Refs. [32,34,51].

Figure 5(c) shows synthetic spectra with the experimental and at a higher resolution calculated with the HULLAC suite of codes for the experimental plasma parameters, $T_e=1.3$ keV, $n_e=1.1\times10^{21}$ cm^{-3}. The HULLAC calculations were performed in the steady state approximation. This comparison is justified because the lithium-like dielectronic satellites closely follow electron temperature changes on time scales less than a 0.1 ns. The intensities of the dominant features, i.e., the He-β_1 and satellite feature 4 agree with the experiment. However, some discrepancies are apparent for the calculated intensities and wavelengths of features 2 and 3. The calculated wavelength of feature 3 is too close to feature 4

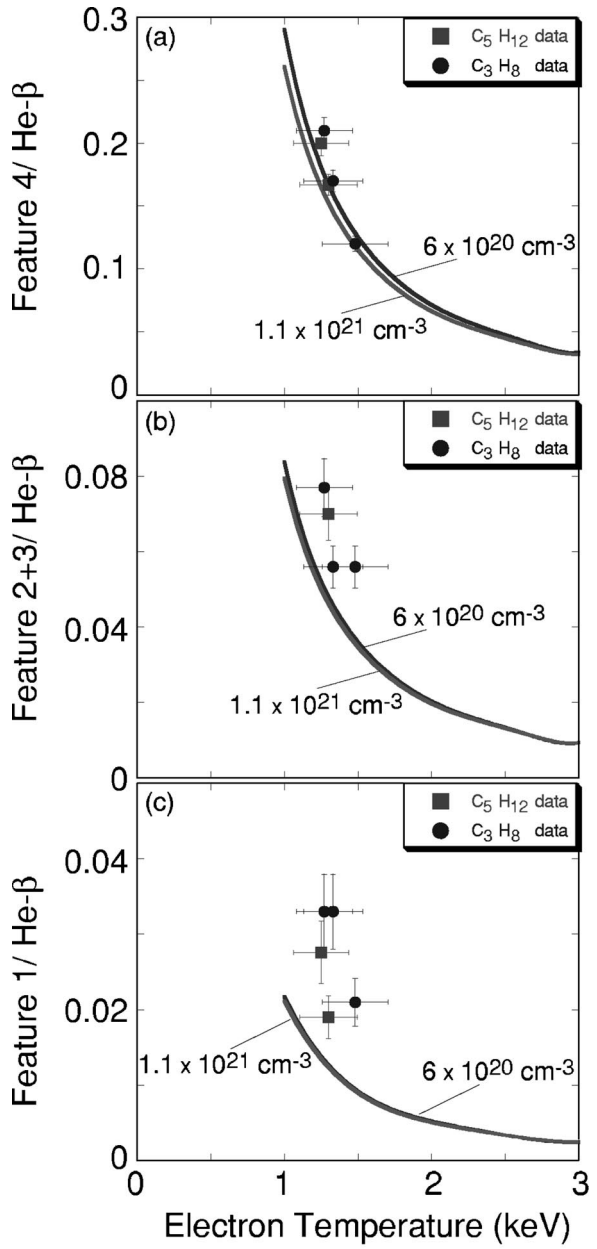

FIG. 6. Comparison between the experimental line ratios from C_3H_8-filled ($n_e = 6\times10^{20}$ cm^{-3}) and C_5H_{12}-filled ($n_e = 1.1\times10^{21}$ cm^{-3}) gas bags with steady-state kinetics (collisional-radiative) model calculations. The intensity ratio between the He $-\beta$ transition (resonance plus intercombination line) to satellite feature 4, which upper state is populated by dielectronic capture, shows excellent agreement with the modeling (a). The ratio between the He$-\beta$ line and feature 2 (capture satellite) plus feature 3 (collisional excited satellite) shows marginal agreement (b) while noticeable discrepancies can be seen for the purely collisional excited satellite feature 1 over the He-β line (c).

(this is also true when compared with the high resolution experimental data of Refs. [32,34]), and the sum of the intensity of feature 2 and feature 3 is smaller than observed in the present experiment [cf. Fig. 5(b)].

For a more quantitative comparison, we fit the experimental data with a multi-Gaussian profile using a least-squares method. An example is given in Fig. 5 as the straight black line through the experimental spectrum (shown in gray). We obtain an estimate for the error bar of the experimental intensities of the various spectral lines by varying the fit within the noise of the data. It is in the range of 5% for the intense transitions (e.g., feature 4) to 20% for the weak transitions (e.g., feature 1). In Fig. 5, the $n=3$ dielectronic satellites at 0.3381 nm have not been included in the fit since we do not compare it to modeling. However, we have verified by fitting the $n=3$ feature with a single line that they do not influence the intensity of the He-β_2 line. Furthermore, we expect the intensities of satellites with increasing principal quantum number of the spectator electron ($n=4$, etc.) to be negligibly small. These satellites are too close to the resonance line to be resolvable with the present spectrometer. It was shown in Ref. [16], that with increasing nuclear charge Z, dielectronic satellites with $n>2$ spectator electrons become less important. According to Gabriel for $Z>14$, the contribution of the $n=3$ dielectronic satellites to the resonance line have become negligible. In the present study the $n=3$ satellites are intense enough so that we can measure their magnitude independently, however these satellites are small enough to indicate that the $n\geqslant4$ satellites make a negligible contribution to the line intensity.

Figure 6 shows the intensity ratio of the various experimental Li-like dielectronic satellites to the He-β transition as a function of the measured electron temperature together with the results of the HULLAC calculations for the two different electron densities: $n_e = 6\times10^{20}$ cm^{-3} for C_3H_8 filled gas bags and $n_e = 1.1\times10^{21}$ cm^{-3} for C_5H_{12} filled gas bags. In Fig. 6(a), feature 4 / He-β, a pure dielectronic capture satellite to resonance line intensity ratio, shows excellent agreement between the experimental data and the kinetics modeling. Since the experimental error bar of this line ratio is the smallest one, i.e., 5%, it can be used for a comparison with various atomic physics calculations. Table I lists the ratios for the experimental temperatures and densities together with calculations using the fully collisional-radiative HULLAC modeling as well as calculations after Eq. (12) using atomic data as discussed in Sec. IV. This comparison shows that the HULLAC calculations agree on average to within 6% with the experiment while the simplified calculations overestimate the experimental ratio by 12% –22%.

While the comparison of the atomic calculations with the experimental dielectronic capture satellite intensities suggest that all the atomic models are close to the experimental data, we find that inner-shell collisional excited satellite lines are not well modeled. Figure 6(b) shows the ratio of the sum of feature 2 and feature 3 to the He-β transition. It is an intermediate case as it adds dielectronic capture satellites and inner-shell collisional excited satellites. In the final comparison Fig. 6(c) shows the ratio of feature 1, derived from purely collisional excited satellites to the He-β transition. Thus, we observe from Fig. 6, a gradually increasing disagreement between the experimental and calculated HULLAC ratios with increasing contribution of collisional excited satellites. Since these ratios are all inferred simultaneously from the same spectra they indicate that electron collisional excited satellites are not well modeled compared to the dielectronic capture satellites, and in the particular case of feature 1 the calculated ratios are outside of the error bars of the experiment.

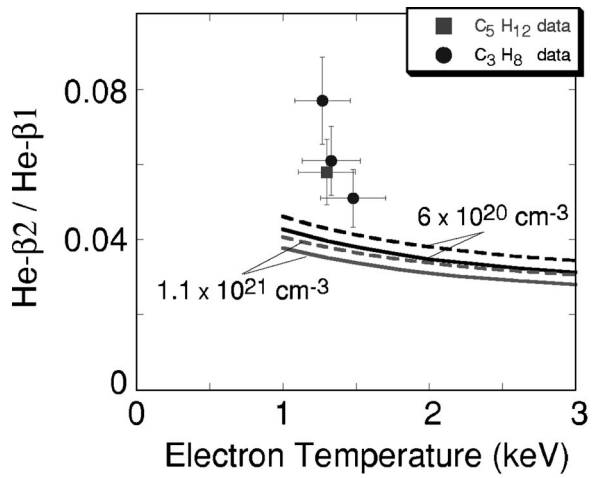

FIG. 7. Comparison between the experimental line ratio of the resonance (He$-\beta_1$) and intercombination line (He-β_2) from C_3H_8-filled ($n_e=6\times10^{20}$ cm^{-3}) and C_5H_{12}-filled ($n_e=1.1\times10^{21}$ cm^{-3}) gas bags with steady-state kinetics (collisional-radiative) HULLAC calculations shown as straight lines. Also shown are calculations using atomic data of Ref. [54] (dashed curves). Discrepancies in the range of a factor 1.3–2 are observed similar to results from low-density tokamak plasmas.

For the comparisons between the ratios determined experimentally and through atomic physics kinetics modeling, we have assumed a Maxwellian electron velocity distribution function. However, we know that for gas bag plasmas, hot electrons are produced by stimulated Raman scattering (SRS) from the heater beams. The SRS losses are constant during the period 0 ns$<t<$0.5 ns [47]. Furthermore, it is also known that hot electrons are a secondary product of SRS [12,52]. To test the hypothesis that the Maxwellian velocity distribution yields the correct kinetics, calculations including a modification of the velocity distribution by suprathermal (hot) electrons have also been performed. For the time of the x-ray spectroscopic measurements, the hot electron fraction is inferred to be constant at the 3% level [12]. This value is consistent with time-integrated measurements of the bremsstrahlung in the x-ray spectral region with calibrated diodes [53] giving a time-integrated fraction of 1% and a hot electron temperature of 17 keV [22].

To ascertain the potential effects of the hot electrons we use time-dependent calculations to model the experimental conditions described above. These calculations show that hot electrons increase the collisional excitation and therefore the intensity of the He-β transition as well as the inner-shell collisional excited satellites only for times $t<0.1$ ns. This is because at these early times the fraction of He-like ions is negligibly small so that inner-shell excitation of Be- and Li-like ions by hot electrons is important. However, at later times when the spectra have been measured, i.e., 0.3 ns $<t<0.5$ ns, the effect of the hot electrons is found to be negligible because He-like ions begin to dominate the charge state distribution so that thermal electrons dominate the collisional excitation process.

These calculations rule out the possibility that inner-shell collisional excited satellite intensities are influenced by hot electrons, leaving the most likely explanation for the observed discrepancies to be errors in the atomic kinetics models. These discrepancies most likely arise from differences in the ion balance between model and experiment. Despite remaining discrepancies, the good agreement between the experimental dielectronic capture satellites and the HULLAC calculations suggests that HULLAC is a more appropriate code for the construction of the kinetics models of the He-β complex from high density plasmas than previously used codes. For example, the temperatures of $\sim$800 eV, inferred previously for ICF capsule implosions using the He-β complex [14], which are not in agreement with 2D radiation-hydrodynamic simulations may be themselves in error. In light of the present study it appears that the intensities of the satellites may be underestimated with respect to the He$-\beta$ transition by the kinetics modeling used in Ref. [14].

B. Intercombination line

Although the relative intensity of the intercombination line, He-β_2, is small compared to the resonance transition, He-β_1, we were able to extract the line intensity ratio of both spectral lines with an error of about 20% by our fitting procedure assuming the same line profile for both components. This ratio is shown in Fig. 7 as a function of the electron temperature for the various measured spectra together with the HULLAC calculations. Interaction between the upper levels of these two transitions is discussed in Ref. [34]. In addition, we show kinetics calculations using atomic data of Ref. [54] that have been used previously in Ref. [55]. We find that the calculations underestimate the experimental ratios by a factor of 1.5–2 and are clearly outside the experimental error bars. Using the atomic data of Ref. [54] results only in marginal improvements.

This result does not agree with the previous collisional-radiative modeling of Ref. [55] where the ratio has been found to increase with increasing electron density. Our modeling shows the opposite, namely that this ratio is decreasing for densities above 10^{20} cm^{-3} due to a reduction of the population density of the $1s3p\ ^3P_1$ state by electron collisions. The radiative decay rate of the triplet level is much smaller than that of the singlet level. With increasing electron densities the collisional depopulation rate of the triplet level assumes the same order as its radiative decay rate. Hence, the relative upper state population and relative intensity of the intercombination line decreases compared to the resonance line whose upper level is predominantly depopulated by radiative decay. We note further that, our finding is consistent with other works, e.g., Refs. [56,57], and a study of the discrepancy in Ref. [55] is warranted.

Discrepancies between measured and modeled intercombination line intensities have also been observed previously for the He-β transition [32]. Although it will be interesting to compare the various kinetics codes to understand why this discrepancy occurs, this diagnostic ratio is not of importance since the intensity of the intercombination line is among the smallest of the detectable spectral lines in the spectrum of helium-like argon.

VI. CONCLUSIONS

Experiments in gas bag plasmas with independent T_e and n_e measurements have shown that collisional radiative (kinetics) modeling of the intensities of the He-β line and its dielectronic capture satellites is generally in agreement with

the measured spectra. On the other hand, for the particular case of Li-like satellites arising from inner-shell electron collisional excitation we find discrepancies of up to a factor of two between experiment and kinetics models. Similar discrepancies have also been found in comparisons for the intercombination line whose upper level population is also dominated by collisional processes. We have ruled out possible effects on the inner-shell satellite and intercombination line emission due to plasma gradients, radiative transport, and suprathermal electron excitation leaving errors in the atomic physics modeling to be the most likely explanation.

These experiments became possible due to accurate characterization of these high density plasmas by (ultraviolet) 4ω Thomson scattering [39]. The temperatures from Thomson scattering are in close agreement with the He-α to $jk\not{\ell}$ diagnostic ratio of helium-like argon. Furthermore, the electron temperatures obtained with two different two-dimensional radiation-hydrodynamic codes have also been found qualitatively similar but quantitatively distinct from the Thomson scattering results, but some uncertainties remain due to the inherent three-dimensional geometry of the experiment.

The determination that there are problems with the collisionally populated states is important for the interpretation of inertial confinement fusion capsule implosions where electron densities and temperature have been measured using the spectral line shape of the He-β transition of Ar XVII. The analysis of the implosion data has required Stark broadening calculations coupled to a kinetics model to calculate the detailed line intensities and widths. Our experiments suggest that the code HULLAC might be more suitable to calculate the level population kinetics than previously used codes. HULLAC results in higher temperatures for the implosion conditions of Ref. [14] in closer agreement with the 2D radiation hydrodynamic modeling and other spectroscopic techniques. These results indicate that benchmarking kinetics codes with Thomson scattering is an important area in present ICF research. Given the verification of the Thomson scattering technique presented here, it is clear that the ablation plasma conditions created in hohlraums can be determined in the future with accuracy shedding light on the crucial x-ray ablation process.

ACKNOWLEDGMENTS

This work was performed under the auspices of the U.S. Department of Energy by University of California Lawrence Livermore National Laboratory under Contract No. W-7405-ENG-48. The authors would like to thank Professor U. Safronova for sending satellite dielectronic recombination strengths and Dr. J. K. Nash for helpful discussions regarding the atomic data used in the models of Ref. [14].

[1] B. Yaakobi, D. Steel, S. E. Thorsos, A. Hauer, and B. Perry, Phys. Rev. Lett. **39**, 1526 (1977); B. Yaakobi, S. Skupsky, R. L. McCrory, C. F. Hooper, H. Deckman, P. Bourke, and J. M. Soures, *ibid.* **44**, 1072 (1980); B. Yaakobi, D. Steel, E. Thorsos, A. Hauer, B. Perry, S. Skupsky, J. Geiger, C. M. Lee, S. Letzring, J. Rizzo, T. Mukaiyama, E. Lazarus, G. Halpern, H. Deckman, J. Delettrez, J. Soures, and R. McCrory, Phys. Rev. A **19**, 1247 (1979).

[2] K. B. Mitchell, D. B. vanHulsteyn, G. H. McCall, P. Lee, and H. R. Griem, Phys. Rev. Lett. **42**, 232 (1979).

[3] A. Hauer, K. B. Mitchell, D. B. van Hulsteyn, T. H. Tan, E. J. Linnebur, M. Mueller, P. C. Kepple, and H. R. Griem, Phys. Rev. Lett. **45**, 1495 (1980).

[4] M. H. Key, J. G. Lunney, J. D. Kilkenny, and R. W. Lee, Appl. Phys. Lett. **36**, 269 (1980).

[5] C. F. Hooper, Jr., D. P. Kilcrease, R. C. Mancini, L. A. Woltz, D. K. Bradley, P. A. Jaanimagi, and M. C. Richardson, Phys. Rev. Lett. **63**, 1267 (1989); C. F. Hooper, Jr., L. A. Woltz, R. C. Mancini, N. D. Delamater, M. C. Richardson, and R. L. Kauffman, J. Quant. Spectrosc. Radiat. Transf. **44**, 79 (1990).

[6] B. A. Hammel, P. Bell, C. J. Keane, R. W. Lee, and C. L. S. Lewis, Rev. Sci. Instrum. **61**, 2774 (1990); B. A. Hammel, C. J. Keane, M. D. Cable, D. R. Kania, J. D. Kilkenny, R. W. Lee, and R. Pasha, Phys. Rev. Lett. **70**, 1263 (1993); B. A. Hammel, C. J. Keane, T. R. Dittrich, D. R. Kania, J. D. Kilkenny, R. W. Lee, and W. K. Levedahl, J. Quant. Spectrosc. Radiat. Transf. **51**, 113 (1994).

[7] C. J. Keane, B. A. Hammel, D. R. Kania, J. D. Kilkenny, R. W. Lee, A. L. Osterheld, L. J. Suter, R. C. Mancini, C. F. Hooper, Jr., and N. D. Delamater, Phys. Fluids B **5**, 3328 (1993); C. J. Keane, B. A. Hammel, A. L. Osterheld, and D. R. Kania, Phys. Rev. Lett. **72**, 3029 (1994).

[8] H. Nishimura, T. Kisho, H. Shiraga, T. Endo, K. Fujita, H. Takabe, Y. Kato, and S. Nakai, Phys. Plasmas **2**, 2063 (1995).

[9] K. Fujita, Y. Ochi, H. Nishmura, H. Azechi, N. Miyanaga, H. Shiraga, I. Uschmann, M. Vollbrecht, E. Förster, and A. Sunahara, J. Quant. Spectrosc. Radiat. Transf. **58**, 585 (1997).

[10] D. K. Bradley, J. A. Delettrez, R. Epstein, R. P. J. Town, C. P. Verdon, B. Yaakobi, S. Regan, F. J. Marshall, T. R. Boehly, J. P. Knauer, D. D. Meyerhofer, V. A. Smalyuk, W. Seka, D. A. Haynes, M. Gunderson, G. Junkel, C. F. Hooper, P. M. Bell, T. J. Ognibene, and R. A. Lerche, Phys. Plasmas **5**, 1870 (1998).

[11] C. A. Back, D. H. Kalantar, R. L. Kauffman, R. W. Lee, B. J. MacGowan, D. S. Montgomery, L. V. Powers, T. D. Shepard, G. F. Stone, and L. J. Suter, Phys. Rev. Lett. **77**, 4350 (1996); C. A. Back, S. H. Glenzer, R. W. Lee, B. J. MacGowan, J. C. Moreno, J. K. Nash, L. V. Powers, and T. D. Shepard, in *Atomic Processes in Plasmas*, edited by A. Osterheld and W. Goldstein, AIP Conf. Proc. No. 381 (AIP, New York, 1996), pp. 123–130.

[12] S. H. Glenzer, F. B. Rosmej, R. W. Lee, C. A. Back, K. G. Estabrook, B. J. MacGowan, T. D. Shepard, and R. E. Turner, Phys. Rev. Lett. **81**, 365 (1998); S. H. Glenzer, in *Spectral Line Shapes*, edited by R. M. Herman, AIP Conf. Proc. No. 467 (AIP, New York, 1999), pp. 49–63.

[13] M. D. Cable, S. P. Hatchett, J. A. Caird, J. D. Kilkenny, H. N. Kornblum, S. M. Lane, C. Laumann, R. A. Lerche, T. J. Murphy, J. Murray, M. B. Nelson, D. W. Phillion, H. Powell, and D. B. Ress, Phys. Rev. Lett. **73**, 2316 (1994).

[14] N. C. Woolsey, A. Asfaw, B. Hammel, C. Keane, C. A. Back, A. Calisti, C. Mosse, R. Stamm, B. Talin, J. S. Wark, R. W. Lee, and L. Klein, Phys. Rev. E **53**, 3696 (1996); N. C. Woolsey, B. A. Hammel, C. J. Keane, A. Asfaw, C. A. Back, J. C.

Moreno, J. K. Nash, A. Calisti, C. Mosse, R. Stamm, B. Talin, L. S. Klein, and R. W. Lee, *ibid.* **56**, 2314 (1997); **57**, 4650 (1998); J. Quant. Spectrosc. Radiat. Transf. **58**, 975 (1997).

[15] H. R. Griem, *Spectral Line Broadening by Plasmas* (Academic, New York, 1974).

[16] A. H. Gabriel, Mon. Not. R. Astron. Soc. **160**, 99 (1972).

[17] R. W. Lee, B. L. Whitten, and R. E. Strout II, J. Quant. Spectrosc. Radiat. Transf. **32**, 91 (1984).

[18] R. C. Mancini, C. F. Hooper, N. D. Delamater, A. Hauer, C. J. Keane, B. A. Hammel, and J. K. Nash, Rev. Sci. Instrum. **63**, 5119 (1992); D. A. Haynes, D. T. Garber, C. F. Hooper, R. C. Mancini, Y. T. Lee, D. K. Bradley, J. Delettrez, R. Epstein, and P. A. Jaanimagi, Phys. Rev. E **53**, 1042 (1996).

[19] G. Zimmerman and W. Kruer, Comments Plasma Phys. Control. Fusion **2**, 85 (1975).

[20] Y. Ochi, K. Fujita, I. Niki, H. Nishmura, N. Isuni, A. Sunahara, S. Naruo, T. Kawamura, M. Fukao, H. Shiraga, H. Takabe, K. Mima, S. Nakai, I. Uschmann, B. Butzbach, and E. Förster, J. Quant. Spectrosc. Radiat. Transf. (in press).

[21] D. H. Kalantar, B. J. MacGowan, T. P. Bernat, D. E. Klem, W. W. Hsing, and B. Failor, Rev. Sci. Instrum. **66**, 782 (1995); D. H. Kalantar, D. E. Klem, B. J. MacGowan, J. D. Moody, D. S. Montgomery, D. H. Munro, T. D. Shepard, G. F. Stone, B. J. Failor, and W. W. Hsing, Phys. Plasmas **2**, 3161 (1995).

[22] B. J. MacGowan, B. B. Afeyan, C. A. Back, R. L. Berger, G. Bonnaud, M. Casanova, B. I. Cohen, D. E. Desenne, D. F. Dubois, A. G. Dulieu, K. G. Estabrook, J. C. Fernandez, S. H. Glenzer, D. E. Hinkel, D. H. Kalantar, R. L. Kauffman, R. K. Kirkwood, W. L. Kruer, A. B. Langdon, B. F. Lasinski, D. S. Montgomery, J. D. Moody, D. H. Munro, L. V. Powers, H. A. Rose, C. Rousseaux, R. E. Turner, B. H. Wilde, S. C. Wilks, and E. A. Williams, Phys. Plasmas **3**, 2029 (1996).

[23] S. H. Glenzer, C. A. Back, K. G. Estabrook, B. J. MacGowan, D. S. Montgomery, R. K. Kirkwood, J. D. Moody, D. H. Munro, and G. F. Stone, Phys. Rev. E **55**, 927 (1997).

[24] A. Bar-Shalom and M. Klapisch, Comput. Phys. Commun. **50**, 375 (1988).

[25] M. Klapisch, Comput. Phys. Commun. **2**, 239 (1971).

[26] M. Klapisch, J. Schwob, B. Fraenkel, and J. Oreg, J. Opt. Soc. Am. **67**, 148 (1977).

[27] J. Oreg, W. H. Goldstein, M. Klapisch, and A. Bar-Shalom, Phys. Rev. A **44**, 1750 (1991).

[28] A. Bar-Shalom, M. Klapisch, and J. Oreg, Phys. Rev. A **38**, 1773 (1988).

[29] U. I. Safronova (private communication), L. A. Vainshtein, and U. I. Safronova, At. Data Nucl. Data Tables **25**, 311 (1980).

[30] M. H. Chen, At. Data Nucl. Data Tables **34**, 301 (1986).

[31] J. Nilsen, At. Data Nucl. Data Tables **38**, 339 (1988).

[32] P. Beiersdorfer, A. L. Osterheld, T. W. Phillips, M. Bitter, K. W. Hill, and S. von Goeler, Phys. Rev. E **52**, 1980 (1995).

[33] V. A. Boiko, S. A. Pikuz, U. I. Safronova, and A. Ya. Faenov, Mon. Not. R. Astron. Soc. **185**, 789 (1978).

[34] J. E. Rice, K. B. Fournier, U. I. Safronova, J. A. Goetz, S. Gutmann, A. E. Hubbard, J. Irby, B. LaBombard, E. S. Marmar, and J. L. Terry, New J. Phys. **1**, 19.1 (1999).

[35] E. M. Campbell, J. T. Hunt, E. S. Bliss, D. R. Speck, and R. P. Drake, Rev. Sci. Instrum. **57**, 2101 (1986).

[36] C. A. Back, R. L. Kauffman, P. M. Bell, and J. D. Kilkenny, Rev. Sci. Instrum. **66**, 764 (1995).

[37] J. D. Kilkenny, Laser Part. Beams **9**, 49 (1991).

[38] F. Ze, R. L. Kauffman, J. D. Kilkenny, J. Weidwald, P. M. Bell, R. Hanks, J. Steward, D. Dean, J. Bauer, and R. Wallace, Rev. Sci. Instrum. **63**, 5124 (1992).

[39] S. H. Glenzer, W. E. Alley, K. G. Estabrook, J. D. De Groot, M. Haines, J. H. Hammer, J.-P. Jaddaud, B. J. MacGowan, J. D. Moody, W. Rozmus, L. J. Suter, T. L. Weiland, and E. A. Williams, Phys. Plasmas **6**, 2117 (1999); S. H. Glenzer, C. A. Back, K. G. Estabrook, R. Wallace, K. Baker, B. J. MacGowan, B. A. Hammel, R. E. Cid, and J. S. De Groot, Phys. Rev. Lett. **77**, 1496 (1996); S. H. Glenzer, T. L. Weiland, J. Bower, A. J. MacKinnon, and B. J. MacGowan, Rev. Sci. Instrum. **70**, 1089 (1999).

[40] H.-J. Kunze, in *Plasma Diagnostics*, edited by W. Lochte-Holtgreven (North-Holland, Amsterdam, 1968), p. 550.

[41] J. Sheffield, *Plasma Scattering of Electromagnetic Radiation* (Academic, New York, 1975).

[42] E. E. Salpeter, Phys. Rev. **120**, 1528 (1960); J. A. Fejer, Can. J. Phys. **38**, 1114 (1960); J. P. Dougherty, and D. T. Farley, Proc. R. Soc. London, Ser. A **259**, 79 (1960); J. Renau, J. Geophys. Res. **65**, 3631 (1960).

[43] B. D. Fried, R. B. White, and T. K. Samec, Phys. Fluids **14**, 2388 (1971); R. J. Huck and E. A. Johnson, Phys. Rev. Lett. **44**, 142 (1980); E. A. Williams, R. L. Berger, R. P. Drake, A. M. Rubenchik, B. S. Bauer, D. D. Meyerhofer, A. C. Gaeris, and T. W. Johnston, Phys. Plasmas **2**, 129 (1995).

[44] J. A. Fejer, Can. J. Phys. **39**, 716 (1961); D. E. Evans, Plasma Phys. **12**, 573 (1970).

[45] T. Shepard, C. A. Back, D. H. Kalantar, R. L. Kauffman, C. J. Keane, D. E. Klem, B. F. Lasinski, B. J. MacGowan, L. V. Powers, L. J. Suter, R. E. Turner, B. H. Failor, and W. W. Hsing, Rev. Sci. Instrum. **66**, 749 (1995); Phys. Rev. E **53**, 5291 (1996).

[46] R. S. Majoribanks, M. C. Richardson, P. A. Jaanimagi, and R. Epstein, Phys. Rev. A **46**, 1747 (1992); R. S. Majoribanks, F. Budnik, G. Kulcsár, and L. Zhao, Rev. Sci. Instrum. **66**, 683 (1995).

[47] J. D. Moody, B. J. MacGowan, R. L. Berger, K. G. Estabrook, S. H. Glenzer, R. K. Kirkwood, W. L. Kruer, D. S. Montgomery, and G. F. Stone, Phys. Plasmas (to be published).

[48] T. Holstein, Phys. Rev. **72**, 1212 (1947); E. E. Fill, J. Quant. Spectrosc. Radiat. Transf. **39**, 489 (1988).

[49] O. L. Landen, P. M. Bell, J. A. Ortel, J. J. Satariano, and D. K. Bradley, in *Ultrahigh- and High-Speed Photography, Videography, and Photonics* (SPIE, Bellingham, WA, 1993), Vol. 2002, p. 2.

[50] B. L. Henke, E. M. Gullikson, and J. C. Davis, At. Data Nucl. Data Tables **54**, 331 (1993).

[51] P. G. Burkhalter, J. Shiloh, A. Fisher, and R. D. Cowan, J. Appl. Phys. **50**, 4532 (1979).

[52] K. G. Estabrook *et al.*, Phys. Rev. Lett. **45**, 1399 (1980); K. G. Estabrook and W. L. Kruer, Phys. Fluids **26**, 1892 (1983).

[53] C. L. Wang, Rev. Sci. Instrum. **52**, 1317 (1981); H. N. Kornblum *et al.*, Lawrence Livermore National Laboratory, Report No. UCRL-81471, 1978.

[54] F. P. Keenan, S. M. McCann, and A. E. Kingston, Phys. Scr. **35**, 432 (1987).

[55] F. B. Rosmej, Phys. Rev. E **58**, R32 (1998).

[56] V. A. Boiko, S. A. Pikuz, and A. Ya. Faenov, J. Phys. B **12**, 1889 (1979).

[57] E. V. Aglitskii, V. A. Boiko, A. V. Vinogradov, and E. A. Yukov, Sov. J. Quantum Electron. **4**, 322 (1974).